Measurement-Based Equivalent Circuit Model for Time-Domain Simulation of EMI Filters

Simone Negri
Department of Electronics, Information and Bioengineering
Politecnico di Milano
Milan, Italy
simone.negri@polimi.it

Giordano Spadacini
Department of Electronics, Information and Bioengineering
Politecnico di Milano
Milan, Italy
giordano.spadacini@polimi.it

Flavia Grassi
Department of Electronics, Information and Bioengineering
Politecnico di Milano
Milan, Italy
flavia.grassi@polimi.it

Sergio Pignari
Department of Electronics, Information and Bioengineering
Politecnico di Milano
Milan, Italy
sergio.pignari@polimi.it

***Abstract*— In this paper, a methodology to derive equivalent circuits of EMI filters from S-parameters is introduced and discussed. Starting from measured S-parameters and with no need for information on the internal structure of the filter, a rational approximation of the measured frequency responses is derived and equivalent circuits are directly synthesized. The proposed black-box filter models are compatible with SPICE solvers and can be used, in combination with component-level representations of power-electronic equipment, for the prediction of conducted emissions through time-domain simulation. As an example of usage, a CISPR-25 test setup where the EMI filter operates in the presence of an inverter is discussed.**

Keywords*— *Conducted emission (CE), Electromagnetic interference (EMI), EMI filters, power electronics.

I. INTRODUCTION

The availability of powerful electromagnetic and circuit simulation tools is driving a significant change in Electromagnetic Compatibility (EMC) industry practices, where traditional approaches based on trial-and-error are being increasingly replaced by simulations to reduce costs and development time. In this respect, the prediction of conducted emissions (CE) in power-electronic equipment is becoming of particular significance.

Approximated linear behavioural models composed of frequency-dependent impedances and sources are available in literature [1], [2]. Unitedly with circuit representations of line-impedance stabilization networks (LISNs), energy sources, and cables, these frequency-domain techniques provide a valuable tool for CE analysis [2], [4].

Time-domain circuit simulation is more demanding than frequency-domain analysis since detailed models of each component in the converter are required [5], including parasitics, but it pays off by accounting for non-linearity and time-variance typical of electronic equipment. Indeed, bus-bar capacitances and other parasitic parameters can significantly affect CE estimation and generate mode conversion phenomena [6], so that they cannot be neglected in time-domain circuit models. Possible solutions to evaluate those parasitics may be recognized in impedance measurement or 3D electromagnetic solvers [7] .

The prediction of CE via simulations is particularly useful for performance assessment of EMI filters [2]. However, considering commercial products, information provided by manufacturers is not sufficient for this task, being it usually limited to a) circuit topology with nominal values of the circuit components; b) plots of common-mode (CM) and the differential-mode (DM) insertion loss (IL), defined and experimentally determined according to CISPR 17 standard [8]. In fact, circuit representations not including parasitic phenomena are not useful for filter performance prediction, since over a few kHz the impedance is strongly influenced by nonideal behaviour of capacitors and CM chokes and by inductive/capacitive coupling among neighbouring components. In [9], parasitic elements are added to circuit models to introduce the non-ideal behaviour of components in EMI filters. Anyway, this approach is difficult to apply to complex filters, without access to internal components. Full-wave electromagnetic simulation of the internal structure is a feasible option in principle, but requires comprehensive knowledge of the filter (i.e., internal layout, geometry and electrical parts, magnetic properties of ferrites, etc.) [10], which is commonly undisclosed.

On the other hand, IL cannot be used to infer filter models and suffers from inherent limitations even as a performance index. In fact, IL are defined with specific source and load resistance values (50 Ω), not representative of frequency-dependent impedances of real systems. Additionally, linearity is an intrinsic assumption of the frequency domain representations, so that nonlinearity and time-variance of electronic systems cannot be represented.

In order to overcome these issues, a methodology to derive EMI filter circuit representations from the scattering-parameter (S-parameter) matrix measured at the external filter terminals via a Vector Network Analyzer (VNA) has been recently introduced in [11], [12]. Specifically, passive macromodeling techniques [13] allow approximating the frequency-response with rational functions, and an equivalent circuit is directly generated from S-parameters (i.e., without conversion into an admittance representation which would lead to numerical inaccuracy). This approach does not disclose information about the inner structure (components, properties of materials, etc.) and can be used in any CE modelling framework, both in frequency and time domain. In particular, it is compatible with SPICE solvers and gives full potential for time-domain circuit simulation of dc/dc converters as shown in [11].

In this paper, the approach presented in [11] is extended by providing two alternative equivalent circuits, and it is exemplified for the prediction of CE generated by an inverter and measured in a CISPR-25 test setup.

This paper is organized as follows. In Section II, the modelling procedure (S-parameter measurement, rational approximation, and circuit synthesis) is presented, and the

Published version available, DOI 10.1109/EMCEUROPE51680.2022.9901020

obtained model is verified via IL prediction in frequency domain. Section III presents SPICE time-domain simulations of the considered EMI filter circuit model to predict CE generated by an ac/dc converter. Finally, Section IV draws concluding remarks.

II. EMI Filter Modeling Procedure

A. Measurement of the S-parameter Matrix

Firstly, the considered EMI filter frequency response is characterized by S-parameters measurement carried out by a VNA. The filter is assumed to be linear, neglecting saturation effects (e.g., due to dc or low frequency CM currents in CM chokes) [8]. The result of this procedure is an $N_p \times N_p$ S-parameter matrix, where N_p is the number of electric ports of the filter under test. As an example, a four-port EMI filter is considered hereon, as reported in Fig. 1. Electric ports are defined between a wire terminal and a common-ground reference represented by the metallic filter case. Tests were conducted on a commercial EMI filter (model and manufacturer are unessential and undisclosed), which is considered a black box, since (as common for commercial products) its metallic enclosure is sealed and does not allow internal inspection. Information provided by the manufacturer on the internal structure is limited to the basic circuit topology, which is anyway insufficient for accurate modelling [9]. A metallic enclosure hosting the EMI filter, wires, and coaxial connectors is used, as recommended in [8] and shown in Fig. 2. Measurements were carried out by a Keysight ENA E5071C 4-port VNA in the frequency range 10 kHz – 100 MHz.

B. Rational Approximation of the S-parameter Matrix

In order to allow for automatic circuit synthesis, a rational approximation of the frequency-dependent S-parameters is required. In particular, the measured S-parameter matrix **S** must be represented in a pole-residue form

$$\mathbf{S}(s) = \sum_{k=1}^{n} \frac{1}{s - p_k} \mathbf{R}_k + \mathbf{D} + s\mathbf{E} \qquad (1)$$

where $s=j\omega$ is the complex frequency, p_k with $k=1,\ldots,n$ are common sets of n poles, $\mathbf{R}_k$ are residue matrices associated to each pole, and matrices **D** and **E** represent the low-frequency asymptotic behaviour. The representation (1) can be obtained with any suitable numerical method. This is not a simple task, since the desired set of poles and residues is not only required to provide an accurate representation of the measured frequency response, but also to maintain the system passivity [12]. One recognized solution is the Vector Fitting (VF) algorithm [14]-[16]. VF exhibits robustness, efficiency and accuracy. Additionally, VF can be integrated with passivity-check and enforcement techniques. In this work, the rational approximation (1) is obtained by means of the open-source code available in [17], based on [14]-[16].

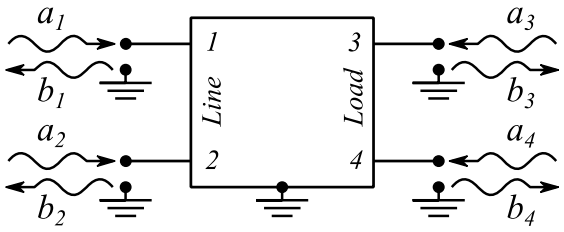

Fig. 1. Definition of ports for S-parameter measurement

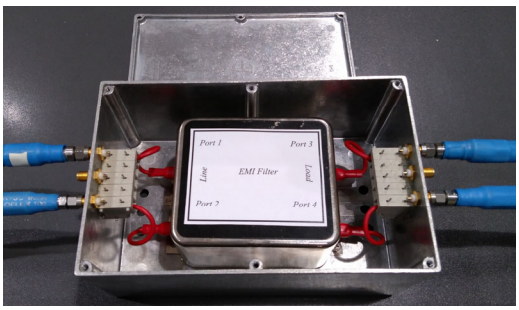

Fig. 2. Test setup for S-parameter measurement (enclosure is opened)

C. Synthesis of an Equivalent Circuit

Once a passive rational approximation (1) of the S-parameter matrix is obtained, several methodologies for automatic circuit synthesis are available in the literature [12]. The simpler approach is to consider the branch-admittance matrix $\mathbf{Y}_B$ of a passive, reciprocal multiport, the elements of which are defined as

$$Y_{B,ii} = \sum_{j=1}^{N_p} Y_{ij} \quad \text{for } i = 1,\ldots,N_p \qquad (2)$$

$$Y_{B,ij} = -Y_{ij} \quad \text{for } i, j = 1,\ldots,N_p \text{ and } i \neq j \qquad (3)$$

These elements can be used to build an equivalent circuit composed of admittances connected between the N_p ports nodes and ground. In particular, $Y_{B,ii}$ (2) represents admittances connected between node i and the common reference ground, while $Y_{B,ij}=Y_{B,ji}$ (3) are admittances connected between nodes i and j. The resulting equivalent circuit of a four-port multiport element is depicted in Fig. 3. Being each admittance expanded in rational form with known poles and residues, a circuit representation of each admittance can be easily obtained with resistors, inductors, and capacitors only, in form of SPICE netlist [18]. In particular, each branch admittance is built with a certain number of parallel-connected branches. The first two branches are one capacitor and one resistor, which correspond to the frequency response asymptotic behaviour. In parallel with those components, one RL branch is added for each real pole, and one RLC branch is added for each complex conjugate pole pair. The resulting branch admittance equivalent circuit is reported in in Fig. 4. Details on how to extract component values can be found in [18].

Unfortunately, this circuit-synthesis technique is not

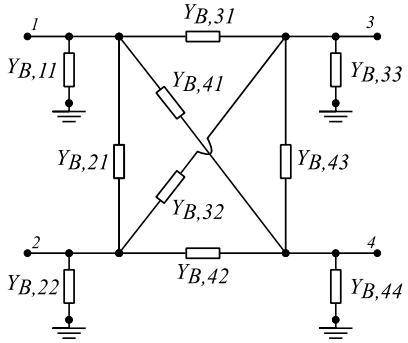

Fig. 3. Equivalent circuit derived from the branch-admittance matrix $\mathbf{Y}_B$ (case $N_p=4$)

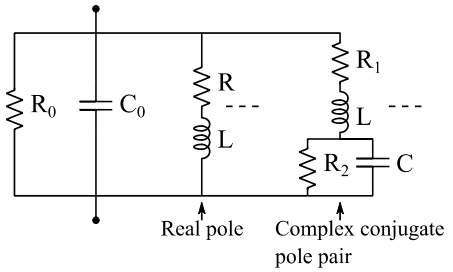

Fig. 4. Equivalent branch admittance circuit

optimal for EMI filters since the conversion from **S** to **Y** introduces numerical issues. Additionally, in EMI filters line-to-ground admittances are usually much larger than line-to-line admittances, which introduces a further source of possible numerical problems. Further discussion is reported in Section II.D, where results obtained directly from **S** and results obtained from **Y** will be compared.

In order to avoid these issues, a method to use S-parameters directly in circuit synthesis is introduced. Differently from literature approaches [12], the proposed technique preserves the idea of the branch-admittance synthesis. This can be obtained considering the formal analogy between admittance and S-parameter representations

$$\mathbf{I}=\mathbf{YV} \Leftrightarrow \mathbf{B}=\mathbf{SA} \tag{4}$$

where **V**, **I** are port voltages and currents vectors, while **A**, **B** are incident and reflected waves vectors. This suggests that the S-parameter matrix **S** can be represented by means of an admittance matrix **Y**, as long as it is fed by voltages and currents numerically equal to the incident and reflected waves. This can be obtained by means of a suitable pair of controlled sources per port, which can be defined considering the relations

$$A_i=\frac{1}{2}\left(V_i+R_0 I_i\right) \tag{5}$$

$$B_i=\frac{1}{2}\left(V_i-R_0 I_i\right) \tag{6}$$

where R_0=50 Ω. In particular, (6) can be represented with a voltage-controlled current source $0.5V_i$ in parallel with a current-controlled current source $-25I_i$, connected to the admittance matrix representing the S-parameters. The physical port voltage can be expressed, combining (5), (6), as:

$$V_i=A_i+B_i \tag{7}$$

which can be represented by means of a voltage-controlled voltage source A_i in series with a current-controlled voltage source B_i at the physical port. This interpretation results in the equivalent circuit shown in Fig. 5, (a) for N_p=4.

Alternatively, (5) is interpreted as a voltage-controlled voltage source $0.5V_i$ in series with a current-controlled voltage source $25I_i$, connected to the admittance matrix representing the S-parameters. The combination of (5) and (6) provides the expression of the physical current as

$$I_i=R_0^{-1}\left(A_i-B_i\right) \tag{8}$$

which is interpreted as a voltage-controlled current source $0.02A_i$ in parallel with a current-controlled current source $-0.02B_i$ at the physical ports. This interpretation results in the equivalent circuit shown in Fig. 5, (b) for N_p=4.

In both representations, the circuit contained in the

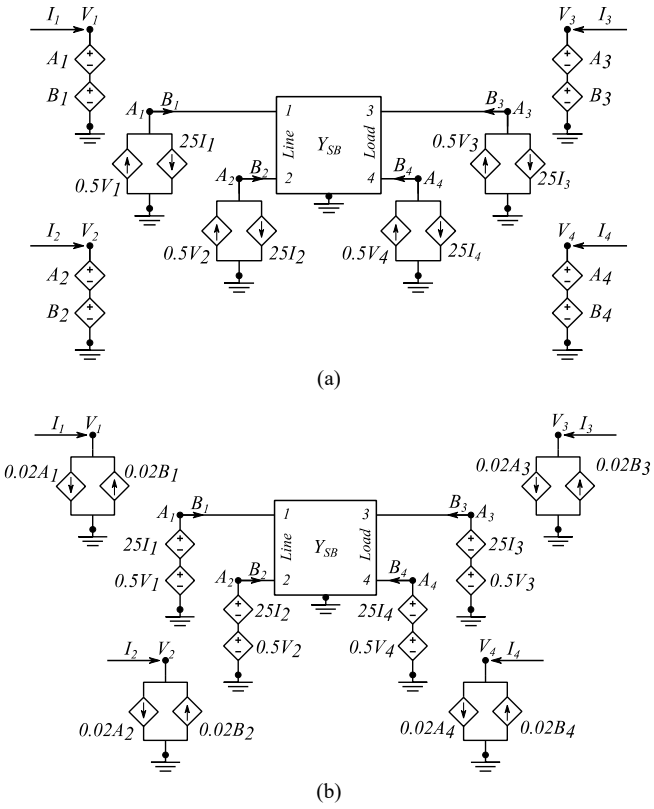

Fig. 5. Two equivalent circuits directly obtained from the scattering-parameter matrix **S** through a formal analogy with the admittance representation.

multiport Y_{SB} reported in Fig. 5 is built as if **S** were an admittance matrix (with units in Siemens) similarly to Fig. 3. Consequently, a fictitious branch-admittance matrix is calculated from the rational approximation of the measured **S** matrix (1), according to

$$\mathbf{Y}_{SB}(s)=\sum_{k=1}^{n}\frac{1}{s-p_k}\mathbf{R}_{SB,k}+\mathbf{D}_{SB}+s\mathbf{E}_{SB} \tag{9}$$

where, similarly to (2), (3),

$$R_{SB,k,ii}=\sum_{j=1}^{N}R_{k,ij},\quad R_{SB,k,ij}=-R_{k,ij} \tag{10}$$

$$D_{SB,ii}=\sum_{j=1}^{N}D_{ij},\quad D_{SB,ij}=-D_{ij} \tag{11}$$

$$E_{SB,ii}=\sum_{j=1}^{N}E_{ij},\quad E_{SB,ij}=-E_{ij} \tag{12}$$

Starting from a rational approximation with 53 poles (23 pairs of complex-conjugate poles and 7 real poles), this procedure leads to an equivalent circuit with $N_p\times(N_p+1)/2$=10 branch admittances. The total number of passive circuit elements amounts to 540 resistors, 240 capacitors, and 300 inductors. Additionally, $4N_p$=16 controlled sources complete the circuit, according to Fig. 5. The SPICE subcircuit netlist realizing the circuit depicted in Fig. 5, (b) is available through IEEE DataPort [12].

D. Comparison between S and Y fitting methods

In order to verify the accuracy of the SPICE model obtained from direct processing of the **S** matrix, a set of frequency-domain simulations is used to predict the filter IL in standard CISPR-17 test setups, using the equivalent circuit reported in Fig. 5, (b). The simulated CM and DM IL in

standard conditions (R_L=R_S=50 Ω) are reported in Fig. 6, where they are compared with actual CISPR-17-compliant measurements. The prediction can be said to be very accurate. with appreciable discrepancy (less than 5 dB) only in a narrow band around 300 kHz, where the CM IL gets it maximum value (90 dB) and solver tolerances slightly affect prediction accuracy. The SPICE models obtained from direct processing of the **S** matrix can be used to predict the IL even with terminal impedances different from 50 Ω, both in frequency [11] and time domain [19].

Considering the numerical issues mentioned in Section II.C, it is of interest to compare these results with the ones obtained from processing of **Y**, which, as mentioned, is obtained from **S**. Regarding the plain fitting process, using 56 poles, the VF algorithm can produce a rational approximation of measured **S** matrix with relative error $\varepsilon < 0.5\%$. With the same number of poles, the rational approximation of the **Y** matrix obtained from the measured **S** matrix has a relative error $1\% < \varepsilon < 2\%$. This is yet indicative of the better performance of direct processing of **S**, but at this stage the conversion to **Y** still produces acceptable results. However, in both cases, the rational model usually needs to be processed to enforce passivity before an equivalent circuit can be derived. In this stage, numerical issues related to **S**-to-**Y** conversion become significant. To highlight this problem, a second set of frequency-domain simulations is used to predict the filter IL in standard CISPR-17 test setups using the model obtained from **Y**. The simulated CM and DM IL in standard conditions (R_L=R_S=50 Ω) are reported in Fig. 7, where they are compared with real CISPR-17-compliant measurements. It is possible to appreciate that there is no agreement between measured and predicted ILs. It would be possible to obtain better results if a much larger number of poles were used (i.e., an equivalent circuit with many more elements, higher computational time) but, anyway, results will hardly be as good as those obtained by direct processing of **S**. The reason is twofold: 1) when converting **S** into **Y**, measurement errors propagate through conversion equations; depending on the real network topology of the device under measurement, it may occur that small measurement errors in the **S** lead to very high errors in the derived **Y**; 2) target quantities of specific interest for EMI filters (CM and DM ILs) are quite sensitive to inaccuracies of admittances in the equivalent circuit topology of Fig. 3. Also, some admittances in Fig. 3 are large, while others are very small (in terms of Siemens), and this magnitude imbalance favours numerical errors. The proposed approach based on fitting the measured **S** matrix and synthesizing the equivalent circuit directly from **S** is a specific contribution of the authors aimed at solving this issue, producing models which are definitely less sensitive to measurement errors and noise.

III. Time-domain Simulation of CE

Once the filter equivalent circuit model has been derived and validated, it can be used in time-domain simulation of CE generated by power electronics converters. Being the latter non-linear, time-varying circuits, time-domain simulations are the only way to correctly predict the generated CE, while frequency-domain simulations require to reduce the converter to a linear model. To exemplify the use of filter equivalent circuit model in time-domain simulations [5]-[7], the SPICE schematic of an half-bridge ac/dc converter in CISPR-25 [20] test setup is reported in Fig. 8. Simulations were performed through LT SPICE, freely available at [21].

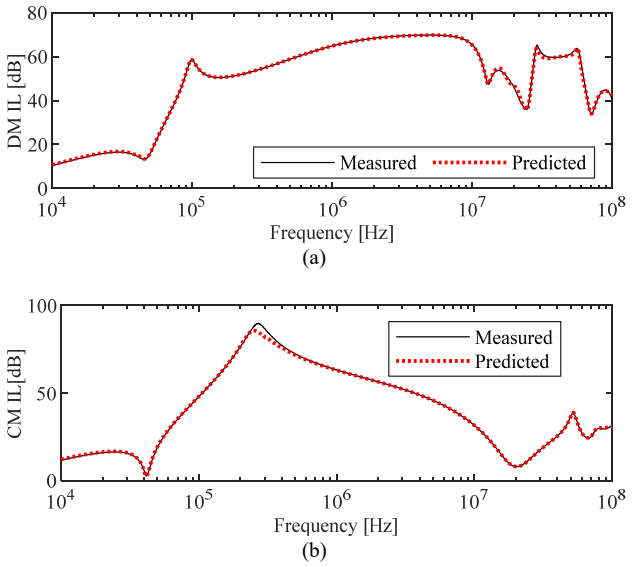

Fig. 6. (a) Symmetrical (DM) and (b) asymmetrical (CM) ILs measured according to CISPR 17 (solid lines) are compared to predictions (dashed lines) obtained from SPICE frequency-domain simulation of the model generated from S matrix fitting.

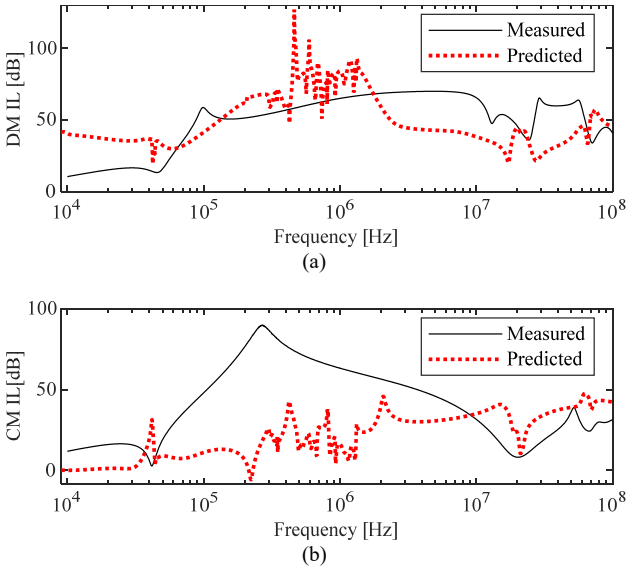

Fig. 7. (a) Symmetrical (DM) and (b) asymmetrical (CM) ILs measured according to CISPR 17 (solid lines) are compared to predictions (dashed lines) obtained from SPICE frequency-domain simulation of the model generated from Y matrix fitting.

In particular, the block U1 contains the subcircuit representing the EMI filter. On the right, elements C1, C11, C12, C13 (dc link capacitors), C14 (capacitive snubber), M3 and M4 (power MOSFET STW11NM80 by STMicroelectronics), D2 and D4 (diode RFN10NS8D by ROHM Semiconductor), L1 (switching inductor), C2 (output filter capacitor) are functional components of the ac/dc converter. The voltage sources V4, V5 drive the gate of M3, M4 and produce a sinusoidal PWM signal with 10 kHz switching frequency of 10 kHz and 0.8 modulation factor. R1 represents a 10 Ω resistive load. Capacitors C7, C8, C9 and C10 represents bus bars capacitances to ground (converter metallic case) and establish a CM path. On the left of the EMI filter, V1 represents a 200 Vdc voltage source, whereas the rest of passive components forms the standard circuit model

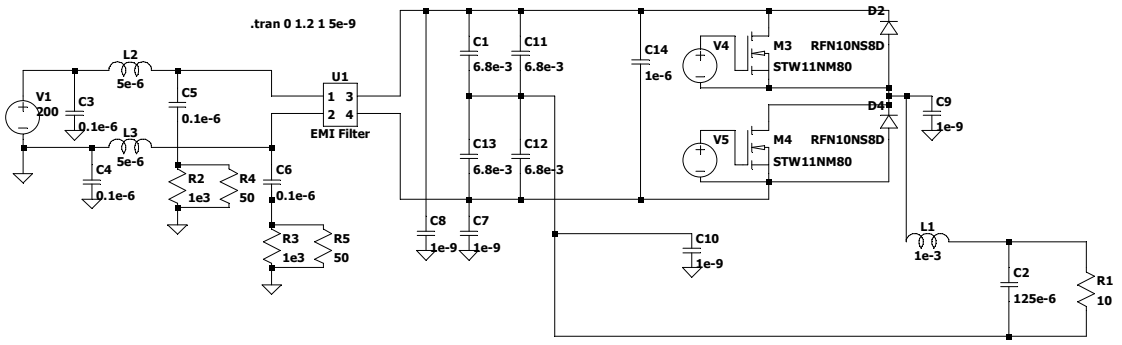

Fig. 8. SPICE schematic (solver [24]) of the CISPR 25 CE test setup, involving an ac/dc converter. The center block represents the subcircuit of the proposed black-box macromodel of the EMI filter.

of the CISPR-25 line-impedance stabilization network (LISN) [20].

For reliable prediction of CE in specific systems, it would be of paramount importance to develop and include broadband models for the converter, the load, cables and bus bars, accounting for dominant parasitic effects [7]. However, for the target of this paper, only the main parasitics have been included, with the only purpose of getting reasonable simulation results. The included parasitics are: series resistance and inductance of dc link capacitors C1, C11, C12, C13 (R_s = 21 mΩ, L_s = 67 nH), snubber capacitor C14 (R_s = 2.7 mΩ, L_s = 94 nH) and output filter capacitor C2 (R_s = 10 mΩ, L_s = 100 nH), series resistance and parallel capacitance of switching inductor L1 (R_s = 10 mΩ, C_p = 1 nF).

Standard CE measures are based on voltages across R4 and R5 for the "+" and "–" dc wire, respectively, which can be directly evaluated by running the SPICE simulation in time domain. The results must be representative of steady-state conditions, which implies that the converter start-up transient should be neglected. The obtained waveforms are hence transformed into the frequency domain by Fast Fourier Transform.

SPICE simulations included two cases: one for the complete circuit in Fig. 8, and a second one without the EMI filter. The obtained CE spectra are reported in Fig. 9 (black and red lines) in terms of CM and DM components of the LISN voltage. In order to get an accurate representation of CE, 100 ms of simulation data have been processed, corresponding to a frequency resolution of 10 Hz. This allows to resolve each peak in the CE spectrum, including fundamental component and harmonics of the sinusoidal PWM signal [22]-[24]. This may be useful in terms of simulations, but it is not comparable with real word measurement, were such a narrow frequency resolution would require unbearably long measures. Consequently, data have been processed by applying the CISPR standard resolution bandwidth (RBW) equal to 200 Hz in the 9 kHz – 150 kHz range and to 9 kHz in the 150 kHz – 100 MHz range [25]. The resulting spectra are reported in Fig. 9 (green and blue lines).

For unfiltered CE (red/blue lines), the DM component prevails in the very low frequency range, where single harmonic groups centred around the integer multiples of the 10 kHz switching frequency are recognizable. Conversely, the CM component is dominant above few hundreds of kHz. Above 150 kHz, the 9 kHz RBW does not allow to resolve each CE peak due to the presence of many harmonic components grouped around integer multiples of the switching frequency, separated only by 50/100 Hz[22]-[24]. Hence CE spectra turn into smooth, continuous lines. This is typical of ac/dc converters, while dc/dc converters with switching frequency larger than the RBW exhibit a different

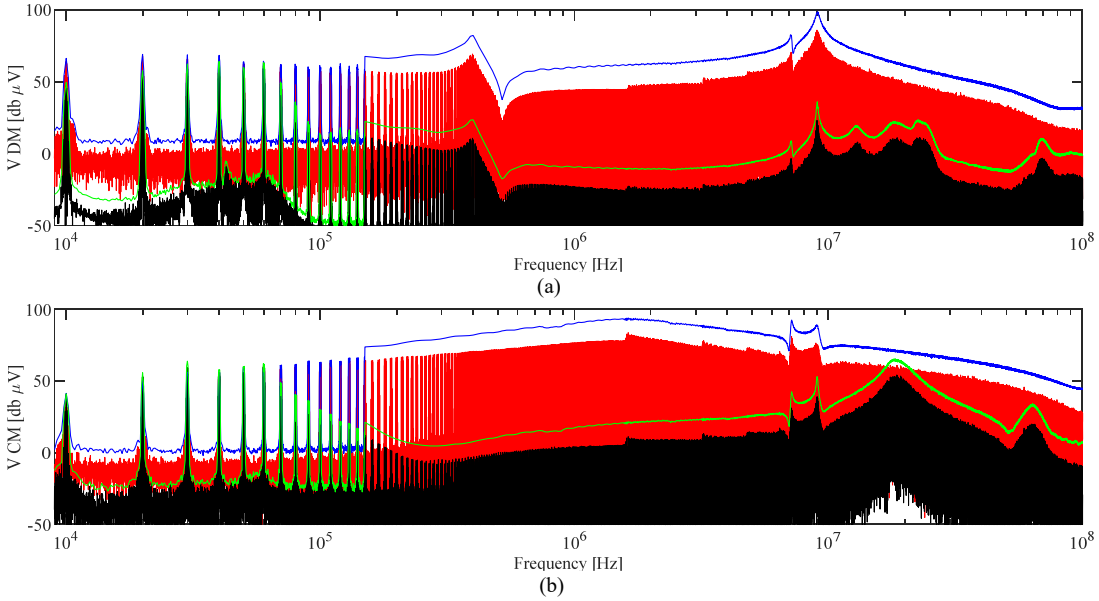

Fig. 9. Predictions of (a) DM and (b) CM CE obtained by SPICE time-domain simulation of the CISPR-25 test setup involving the ac/dc converter in Fig. 8: without EMI filter (red line), without EMI filter, added CISPR RBW (blue line), with EMI filter (black line), with EMI filter, added CIPSR RBW (green line).

behaviour, with single peaks resolved over the whole frequency range, as shown in [9]. This smoothing effect due to RBW is also well known from real word measurement, where EMI receivers apply CISPR RBW by default. Detailed discussion on how to accurately emulate EMI receivers in simulation can be found in [25].

The filtered spectra in Fig. 9 (black/green lines) highlight the suppression characteristics of the considered EMI filter. The attenuation provided by the EMI filter is, however, largely variable over the frequency range and the dependence on the converter operating conditions is not straightforward. This justifies the need for circuit models suitable for time-domain simulation. Indeed, time-domain simulations allow the evaluation of any variation in the converter operating condition (e.g., different modulation factor, source voltage or load) by fast circuit simulations. This solution enables the assessment of the performance of a specific EMI filter regardless of the specific application, which could not be deduced by standard frequency-domain ILs reported in data sheets.

IV. Conclusion

Time-domain simulation of EMI filters is necessary when non-linear and time-varying circuits, such as electronic power converters, are considered. However, EMI filters are usually characterized in terms of frequency-domain quantities, typically S-parameters, which are not easily included in circuit models, and information reported in data sheets is generally insufficient to assess the attenuation of CE through modelling and simulation.

To overcome this limitation and provide an effective and accurate tool to predict EMI filter performance, this paper proposes a methodology to derive equivalent circuit models of EMI filters compatible with circuit solvers like SPICE, and derived from measured S-parameters, with no need for information about the internal filter structure. An illustrative example (ac/dc converter in a CISPR-25 test setup) was presented to highlight the effectiveness of the proposed method in extracting an equivalent circuit suitable for SPICE time-domain simulation of CE.

The proposed modelling technique can be considered as a further step towards virtual prototyping, replacing lengthy trial-and-error approaches. Additionally, since the proposed approach does not oblige to disclose information on the EMI filter internal design, similar models may even be provided by manufacturers as electronic annexes to data sheets, to enable end users to assess and select by simulation the optimal filter for their specific application.

References

[1] Q. Liu, F. Wang, and D. Boroyevich, “Modular-Terminal-Behavioral (MTB) model for characterizing switching module conducted EMI generation in converter systems,” *IEEE Trans. Power Electronics*, vol. 21, no. 6, pp. 1804-1814, Nov. 2006.

[2] A. Perez, A. M. Sanchez, J. R. Regue, M. Ribo, P. Rodriguez-Cepeda, F. J. Pajares, “Characterization of power-line filters and electronic equipment for prediction of conducted emissions,” *IEEE Trans. Electromagn. Compat.*, vol. 50, no. 3, pp. 77-585, Aug. 2008.

[3] H. M. Rebholz, S. Tenbohlen, and W. Kohler, “Time-domain characterization of rf sources for the design of noise suppression filters,” *IEEE Trans. Electromagn. Compat.*, vol. 51, no. 4, pp. 945-952, Nov. 2009.

[4] G. Spadacini, F. Grassi, D. Bellan, S. A. Pignari, and F. Marliani, “Prediction of conducted emissions in satellite power buses,” *Int. Journal Aerospace Engineering*, vol. 2015, pp. 1-10, 2015.

[5] G. Spadacini, F. Grassi, and S. A. Pignari, “Modelling and simulation of conducted emissions in the powertrain of electric vehicles,” *Progress in Electromagn. Res. B*, vol. 69, page 1-15, 2016.

[6] S. Negri, X. Wu, X. Liu, F. Grassi, G. Spadacini and S. A. Pignari, "Mode Conversion in DC-DC Converters with Unbalanced Busbars," *2019 Joint International Symposium on Electromagnetic Compatibility, Sapporo and Asia-Pacific International Symposium on Electromagnetic Compatibility (EMC Sapporo/APEMC)*, Sapporo, Japan, 2019, pp. 112-115.

[7] E. Rondon, F. Morel, C. Vollaire, and J.-L. Schanen, “Modeling of a buck converter with a SiC JFET to predict EMC conducted emissions,” *IEEE Trans. Pow. Electr.*, vol. 29, no. 5, pp 2246-2260, May 2014.

[8] CISPR 17, Methods of measurement of the suppression characteristics of passive EMC filtering devices, IEC, Jun. 2011.

[9] S. Wang, F. C. Lee, and W. G. Odendaal, “Characterization and parasitic extraction of EMI filters using scattering parameters,” *IEEE Trans. Power Electronics*, vol. 20, no. 2, pp. 502–510, 2005.

[10] R. He, Y. Xu, S. Walunj, S. Yong, V. Khilkevich, D. Pommerenke, H. L. Aichele, M. Boettcher, P. Hillenbrand, and A. Klaedtke, “Modeling strategy for EMI filters,” *IEEE Trans. Electromagn. Compat.*, vol. 62, no. 4, pp. 1572-1581, Aug. 2020.

[11] S. Negri, G. Spadacini, F. Grassi and S. A. Pignari, "Black-Box Modeling of EMI Filters for Frequency and Time-Domain Simulations," *IEEE Trans. Electromagn. Compat.,* early access article, pp. 1-10, 2021.

[12] S. Negri, G. Spadacini, F. Grassi, S. A. Pignari, October 27, 2021, "EMI-Filter Black-Box SPICE Model", IEEE Dataport, doi: https://dx.doi.org/10.21227/ydw2-sm33

[13] S. Grivet-Talocia, B. Gustavsen, *Passive Macromodeling Theory and Applications*, 2016, J. Wiley & Sons.

[14] B. Gustavsen and A. Semlyen, “Rational approximation of frequency domain responses by Vector Fitting,” *IEEE Trans. Power Del.*, vol. 14, no. 3, pp. 1052-1061, July 1999.

[15] B. Gustavsen, “Improving the pole relocating properties of vector fitting,” *IEEE Trans. Power Del.*, vol. 21, no. 3, pp. 1587-1592, July 2006.

[16] D. Deschrijver, M. Mrozowski, T. Dhaene, and D. De Zutter, “Macromodeling of multiport systems using a fast implementation of the Vector Fitting method,” *IEEE Microw. Wireless Compon. Lett.*, vol. 18, no. 6, pp. 383-385, June 2008.

[17] B. Gustavsen, *User’s guide for vectfit3,* Available at: https://www.sintef.no/projectweb/vectorfitting/

[18] G. Antonini, “SPICE equivalent circuits of frequency-domain responses,” *IEEE Trans. on Electromagn. Compat.*, vol. 45, no. 3, pp. 502-512, Aug. 2003.

[19] S. Negri, G. Spadacini, F. Grassi and S. A. Pignari, "Prediction of EMI filter attenuation in power-electronic converters via circuit simulation," in *IEEE Trans. on Electromagn. Compat.*, early access, 2022.

[20] CISPR 25, Vehicles, boats and internal combustion engines - Radio disturbance characteristics - Limits and methods of measurement for the protection of on-board receivers, IEC, Oct. 2016.

[21] Linear Technology Inc., *LTspice IV Getting Started Guide*, 2011. Available at: https://www.analog.com/en/design-center/design-tools-and-calculators/ltspice-simulator.html

[22] D. G. Holmes and T. A. Lipo, “Pulse width modulation for power converters – principles and practice”, Wiley Interscience, 2003

[23] S. Negri, S. Barcellona and G. Superti-Furga, "Detailed analysis of harmonic distortion in modular three-phase converters: Analytical and numerical evaluation," *2018 18th International Conference on Harmonics and Quality of Power (ICHQP)*, Ljubljana, 2018, pp. 1-7.

[24] S. Barcellona, S. Negri and G. Superti-Furga, "Space-vector analysis of harmonic distortion in three-phase PWM," *2018 18th International Conference on Harmonics and Quality of Power (ICHQP)*, Ljubljana, 2018, pp. 1-6.

[25] L. Yang, S. Wang, H. Zhao and Y. Zhi, "Prediction and Analysis of EMI Spectrum Based on the Operating Principle of EMC Spectrum Analyzers," in *IEEE Transactions on Power Electronics*, vol. 35, no. 1, pp. 263-275, Jan. 2020.